Int. J. Heat Mass Transfer. Vol. 25, No. 7, pp. 961–973, 1982
Printed in Great Britain

0017-9310/82/070961-13 $03.00/0

HEAT TRANSFER AND PRESSURE DROP CHARACTERISTICS OF ARRAYS OF RECTANGULAR MODULES ENCOUNTERED IN ELECTRONIC EQUIPMENT

E. M. SPARROW, J. E. NIETHAMMER and A. CHABOKI
Dept. Mechanical Engineering, University of Minnesota, Minneapolis, MN 55455, U.S.A.

(*Received* 22 *September* 1981 *and in revised form* 3 *December* 1981)

Abstract—A multi-faceted experimental investigation has been carried out to study heat transfer and pressure drop for airflow in arrays of heat generating rectangular modules deployed along one wall of a flat rectangular duct. Experiments were performed with fully populated arrays, arrays in which there are missing modules, arrays where barriers are implanted to obtain heat transfer enhancement, and arrays in which there is both a missing module and a barrier. For the fully populated array without barriers, row-independent (fully developed) heat transfer coefficients were encountered for the 5th and all subsequent rows. When there is a missing module in the array, the heat transfer coefficients at neighboring modules are increased, with the greatest enhancement (about 40%) occurring when the missing module is just upstream of the module of interest. The enhancement due to side-by-side pairs of missing modules differs very little from that induced by a single missing module. The implantation of a barrier in the array is shown to be an effective enhancement device, with the greatest effect (about a factor of two) being felt in the 2nd row downstream of the barrier but with residual enhancement persisting considerably farther downstream. Under some conditions, the enhancing effects of a missing module and a barrier were found to be mutually reinforcing. Pressure distributions were measured in arrays with and without barriers, and the barrier-induced pressure losses identified.

NOMENCLATURE

A_H,	flow cross-section above modules;
b,	barrier height, Fig. 1;
$\mathscr{D}$,	naphthalene–air diffusion coefficient;
H,	height of flow passage, Fig. 1;
h,	per-module heat transfer coefficient;
h^*	value of h for fully populated array without barriers;
K,	per-module mass transfer coefficient;
K^*,	value of K for fully populated array without barriers;
k,	thermal conductivity;
L,	planform dimension of square module, Fig. 1;
$\dot{m}$,	per-module mass transfer rate per unit area;
Nu,	$= hL/k$, per-module Nusselt number;
Pr,	Prandtl number;
P,	static pressure;
P_{atm},	ambient pressure;
Δp_{incr},	barrier-related incremental pressure loss;
Δp_{row},	per-row pressure drop for baseline case;
Re,	$= \rho VH/\mu$, Reynolds number;
S,	intermodule gap, Fig. 1;
Sc,	Schmidt number;
Sh,	$= KL/\mathscr{D}$, per module Sherwood number;
t,	module thickness, Fig. 1;
x,	axial coordinate measured from beginning of array;
V,	mean velocity, equation (5);
$\dot{w}$	rate of airflow.

Greek symbols

μ,	viscosity;
ν,	kinematic viscosity;
ρ,	density;
ρ_{nw},	naphthalene vapor density at module surface;
ρ_{nb},	naphthalene vapor density in bulk flow;
χ_i,	geometrical parameters.

INTRODUCTION

THE COOLING of electronic equipment continues to be an active branch of heat transfer investigation. This activity is motivated by reliability considerations, by the desire to decrease the transit time of electronic signals, and by the advent of new computer configurations and devices. Reliability revolves about control of the temperature level of critical components, while the transit time is diminished by shorter transmission distances, giving rise to closely positioned components and high densities of dissipated electrical power.

An enormous variety of specific geometries are encountered in the cooling of electronic equipment. Furthermore, the flow passages are frequently of irregular shape, often being bounded by components of various sizes and shapes. As a consequence, the approach toward electronic equipment cooling has included elements of art as well as of science. In particular, owing to flow passage diversities and irregularities, fundamental-type research studies have been less common for electronic equipment cooling

than in other branches of heat transfer investigation.

Despite the aforementioned diversities, it is possible to identify generic cooling problems and related flow passage configurations. These generic problems invite systematic research, with the promise that results of broad applicability will be forthcoming.

The work to be reported here is focused on one of the most commonly recurring generic configurations in electronic cooling. This is the case of forced convection air cooling of an array of rectangular heat-generating modules deployed along one wall of a flat rectangular duct. A schematic diagram of such a configuration, showing both top and side views, is presented in Fig. 1. The top view, which occupies the upper portion of the figure, is actually a portrayal looking into the channel as if the top wall were transparent.

The top view shows the modules to be arranged in a regular pattern. In practice, however, any number of modules may be missing from the array, and the distribution of missing modules is more or less random. Another feature of such a cooling configuration is the presence of barriers which protrude above the plane of the modules. A typical barrier installation is illustrated in both views in Fig. 1. A barrier is intended to function as an enhancement device. It is installed in order to increase the heat transfer coefficient at a module which has a particularly high heat dissipation and/or a crucial temperature limitation.

Missing modules are the rule rather than the exception. Consequently, the effect of missing modules on the heat transfer coefficients at the remaining modules is mainline information—actually of greater practical relevance than the coefficients for the fully populated array (i.e., without missing modules). In this regard, a key issue is the question of how far from a missing module does its influence prevail (either upstream, downstream, or to the side). Similarly, with respect to barriers, it is relevant to identify their range of influence and, in particular, the downstream position at which they induce a maximum value of the heat transfer coefficient. The presence of barriers necessarily increases the pressure drop, and a knowledge of the incremental drop is needed in the assessment of the net worth of the barriers. In general, missing modules and barriers may be simultaneous occurrences, and the extent of their interaction needs to be determined.

The foregoing discussion sets the stage for a description of the multifaceted experimental research program undertaken here. The experiments included the determination of per-module heat transfer coefficients and of the pressure distribution along the array for a wide range of operating conditions.

The first set of experiments was performed using a baseline configuration in which all modules were present and where there were no barriers. Per-module heat transfer coefficients were measured in both the thermal entrance and fully developed regimes. Attention was then focused on the effects of a single missing module on the per-module heat transfer coefficient at positions which are uninfluenced by the entrance region. In this set of experiments, the distance between the missing module and the module whose coefficient was being measured was increased systematically in all directions. This was followed by another set of experiments in each of which a pair of modules was missing and, once again, the distance between the missing pair and the measurement site was varied parametrically.

At this point, attention was turned to the barriers. For each of two barrier heights, per-module heat transfer coefficients were measured in the successive rows downstream of the barrier (and, to a lesser extent, upstream). Then, the case in which there was both a barrier and a missing module was investigated, once again on a per-module, row-by-row basis.

In separate experiments, the pressure distributions were measured for the baseline case (no missing modules, no barriers) and in the presence of barriers of various heights.

The aforementioned measurements were made at each of three Reynolds numbers which are believed to encompass the range of practical applications. To facilitate the experimental work, the heat transfer coefficients were deduced from mass transfer measurements made via the naphthalene sublimation technique.

To convey the results in a readily perceived format, the per-module heat transfer coefficients corresponding to missing modules and/or barriers are ratioed with those for the baseline case (no missing modules, no barriers). The departure of these ratios from one immediately indicates the extent of the enhancement or reduction in heat transfer coefficient.

The authors were unable to find any work in the literature that is comparable to that reported here. The state of the art in electronic cooling, as it existed in 1965, is set out in a book by Kraus [1]. More recent developments are chronicled by Bergles [2].

THE EXPERIMENTS

Experimental apparatus. The array of modules pictured in Fig. 1 was housed in a horizontal, flat rectangular duct whose overall length included, along the flow direction, a module-free inlet section, the test section (site of the modules), and a module-free exit length. The function of the inlet section was to deliver a well defined, reproducible (i.e. fully developed) flow to the initial row of modules in the test section, while the exit length provided an equally well defined and reproducible flow pattern at the last row of modules. Since the host duct was uniform in height all along its length, the free flow area in the test section was smaller (owing to the blockage caused by the modules) than the flow cross-sections upstream and downstream of the array.

Attention will now be focused on the test section. The test section was designed so that its upper wall could be removed and reset in place in a matter of

seconds, thus enabling the rapid access to the array of modules that is necessary for the efficient use of the naphthalene sublimation technique. When in place the upper wall was secured by six heavy-duty, quick-acting clamps and was sealed against leaks with O-ring material.

The array was laid out in a regular pattern as illustrated in Fig. 1, with the barriers being an optional feature, either present or absent as desired. In plan view (i.e. Fig. 1) each module is a square and, furthermore, the transverse and longitudinal intermodule gaps are identical. There are four length dimensions which define the geometrical characteristics of the array and its relationship to the flow passage. These include the module planform dimension L and the module thickness t, the intermodule gap S and the height H of the flow passage between the module and the opposite wall of the channel. Although there is a tendency to deal with dimensional quantities in connection with electronic equipment cooling, the use of dimensionless parameters is preferable because they accord greater generality to the results. For the present experiments, the dimension ratios defining the array and its related flow passage are

$$t/L = \tfrac{3}{8},\ S/L = \tfrac{1}{4},\ (H + t)/L = 1. \quad (1)$$

These dimension ratios were chosen to closely correspond to a recurring practical cooling configuration.

The barriers used here fitted snugly into the gap between the rows of modules. Two barrier heights b were employed in the heat (mass) transfer experiments, with the heights specified by

$$b/(t + H) = \tfrac{1}{2} \text{ and } \tfrac{5}{8}. \quad (2)$$

From (1) and (2), it follows that the relative blockage of the flow passage height H due to the barrier is

$$(b - t)/H = \tfrac{1}{5} \text{ and } \tfrac{2}{5}. \quad (2a)$$

Pressure drop studies were also performed for a taller barrier characterized by $(b - t)/H = \tfrac{3}{5}$, but the pressure losses were found to be too great to warrant study of the heat (mass) transfer characteristics.

The test section encompassed seventeen rows of modules. The spanwise extent of the array was more or less as pictured in Fig. 1, with three full-size modules flanked on both ends by a half module. Each half module interfaced with the adjacent side wall of the host duct. The idea underlying the use of the half modules was to more closely model an infinitely wide array, and the success of this approach was verified by comparison of the heat (mass) transfer coefficients at the three full-size modules in a given row. For a fully populated array (no missing modules), spanwise uniformity was within 2%, which corresponds to the reproducibility of the data at a given module.

Two types of modules were employed to populate the test section. Both types were of identical dimensions and of high surface quality and were, therefore, identical from the standpoint of the fluid flow. The two types differed in the materials from which they were fabricated. Brass modules, fabricated to close tolerances (0.001–0.002 in) with a vertical milling machine, were the main occupants of the array. There was no mass transfer at these modules, but their presence created the fluid flow pattern whose effect at a preselected module site was the focus of the investigation. A mass transfer active module, made of naphthalene by a casting process (to be described shortly), occupied the particular site of interest in a given data run.

The use of a single mass transfer module in each data run is entirely sufficient to extract the desired results. This is because all of the interesting phenomena associated with missing modules and barriers are related to the pattern of fluid flow, which is uninfluenced by whether the modules are of brass or naphthalene. An enormous simplification resulted for the use of a single mass transfer module per run, and this enabled efforts to be directed toward examining a wide range of positions of missing modules and barrier-influenced modules.

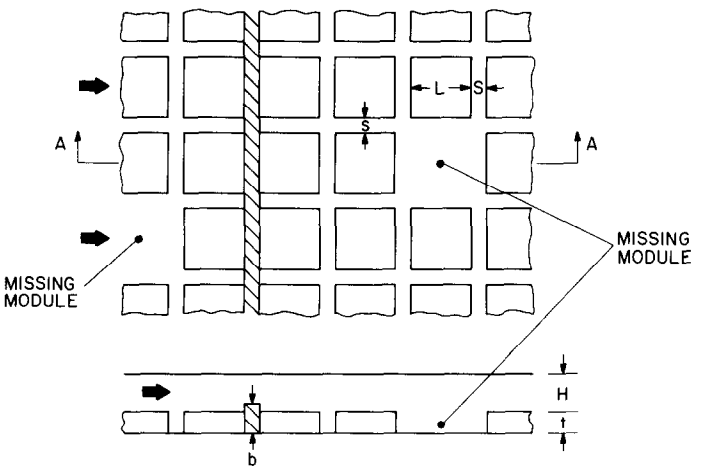

FIG. 1. Array of rectangular modules deployed along one wall of a flat rectangular duct.

The mass transfer module was positioned in its site in the test section with the aid of a gridwork of pencil lines that had been ruled on the duct floor. Careful visual observations showed that even at the highest velocities investigated, there was no displacement whatsoever of the module due to wind forces. The brass modules were passive with respect to the mass transfer measurement procedure (i.e. they were not implanted and later removed and later removed for weighing, as was the naphthalene module). Therefore, it seemed appropriate to fix these modules securely to the duct floor. This was accomplished by a pair of pins which emanated from the bottom of each module (a single pin for the half modules) and mated with corresponding holes in the floor of the duct.

Additional information about the test section and the experimental apparatus will now be conveyed. Thus far, only dimensionless ratios have been specified, equations (1) and (2). With these equations, all test section dimensions can be deduced when only one dimension is specified—$L = 2.667$ cm (1.05 in). The lengths of the inlet, test, and exit sections of the host rectangular duct were 165, 56 and 48 cm (65, 22 and 19 in). The host duct had been fabricated from 0.95 cm ($\frac{3}{8}$ in) aluminum plate, and its internal surfaces (i.e. those which contacted the airflow) had been sanded to a high degree of smoothness.

During the experiments, air was drawn into the inlet section from the laboratory room. The air traversed the test and exit sections of the host rectangular duct, from which it passed through a rectangular-to-circular transition piece which successively led to a flow-metering station (either of two specially calibrated orifices), a control valve, and then to the blower. The blower was situated in a service corridor outside the laboratory, and its exhaust was vented outdoors.

The operation of the system in the suction mode and the placement of the blower outside the laboratory, together with the controlled room temperature, enabled the attainment of steady operating temperatures in the test section. Also, the outside exhaust, coupled with strict handling procedures, ensured that the laboratory was free of naphthalene vapor.

The instrumentation will be discussed shortly along with the experimental procedure.

Naphthalene modules. The fact that all six surfaces of the naphthalene module have to be smooth and true—the bottom as well as the five faces exposed to the airflow — required that an innovative fabrication procedure be devised. A casting procedure based on a special mold was developed. A top view schematic of the mold is shown in Fig. 2, where the base plate, the side walls, and the backstop bars which position the side walls are identified. The square, speckled region is the mold cavity; the top plate, not shown, is similar in size to the base plate. All mold parts were of brass, and those surfaces which bounded the mold cavity were highly polished.

To begin the casting, molten naphthalene was poured into the open mold cavity until it was about

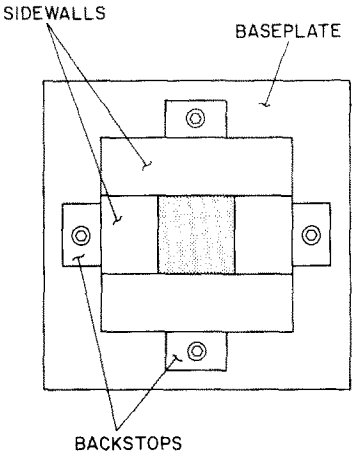

FIG. 2. Top view of mold for casting naphthalene modules (the top plate of the mold is not shown).

three-quarters filled. Then, when the exposed surface just began to skin over, additional naphthalene was poured to a level just even with the height of the mold. The top of the mold was then set in place, and the mold turned over. By this, naphthalene was caused to solidify against the top (now the bottom). In fact, a smooth solidified surface was produced adjacent to all of the walls of the mold.

The solidified naphthalene module was readily unmolded by lateral motions of the top plate and side walls. Once unmolded, the module was grasped with lint-free tissue and loose naphthalene particles wiped away. The module was then wrapped in impermeable plastic wrap and placed in the laboratory to begin the thermal equilibration process. Normally, at least half a dozen modules were produced during a casting session (a freshly cast module was used for each data run).

The modules, once fabricated, were never touched with the fingers. For weighing and installation (removal) in (from) the test section, the module was grasped with modified surgical forceps whose jaws were covered with Teflon shrinkfit tubing.

Instrumentation and procedure. The key instrument for the mass transfer experiments was an ultra-precision Sartorius electronic analytical balance capable of resolving 10^{-5}g (typical mass transfers were 0.02–0.05 g/data run). The temperature of the air entering the duct was sensed with a specially calibrated copper–constantan thermocouple which was read and recorded periodically during a data run by a Doric Digitrend 210 digital voltmeter; the thermocouple readings were backed up by a 0.1°F ASTM-certified thermometer. Test section airflow rates were measured with the aforementioned calibrated orifice plates in conjunction with a water manometer (deflections were always sufficiently large so that reading errors were negligible).

To facilitate the pressure drop studies, the host duct was equipped with a line of 23 pressure taps along its spanwise centerline. The signals from these taps were conveyed via plastic tubing to a pressure selector

switch, the output of which was delivered to a Baratron solid state capacitance-type pressure meter capable of resolving 10^{-4} Torr. The voltage signal from the Baratron was read, averaged, and recorded by a Fluke 2240 C scanning, integrating data logger.

To initiate a mass transfer data run, the test section was arranged to conform to the desired configuration [e.g. module(s) removed and/or barrier installed]. In addition, the site at which the mass transfer module was to be installed was made available by removing the brass module situated there. Then, the plastic-wrapped naphthalene modules to be used during the day's experiments were placed in the test section, with that for the first run set in its proper site and the others placed downstream of the last row. The blower was activated and as it came to steady state, the modules attained thermal equilibrium with the air (about an hour was allowed for the equilibration). About 2 min before the end of the equilibration period, the naphthalene block at the test site was unwrapped, brushed free of any loose particles, and returned to the test section for a brief exposure to the airflow (to ensure the complete removal of loose particles).

Then, with the blower turned off, the module was removed from the test section (using the modified forceps), placed in a special Teflon-lined carrying box and transported to the analytical balance, where it was weighed.

Subsequent to weighing, the module was returned to the test section site, and the duct cover was closed and sealed. The airflow was then initiated and since the control valve had been preset and the blower preheated, the desired flow rate was rapidly attained. During the data run, the temperature, airflow rate, and barometric pressure were monitored and recorded. The run was concluded by deactivating the airflow, removing the naphthalene module from the test section, and weighing it.

At this point, a supplementary data run was carried out to determine a correction for any extraneous mass transfer that might have occurred in the period between the first and second weighings. All of the steps that had been performed between the two weighings were repeated, but the blower was never turned on. A third weighing was then made, and this yielded a correction factor in the $1-1\frac{1}{2}\%$ range.

The pressure drop measurements were made in runs separate from those for mass transfer. The instrumentation for the pressure runs has already been described, and no further elaboration of the experimental procedure need be given here.

DATA REDUCTION

The procedures used to evaluate the per-module heat (mass) transfer coefficient, the Reynolds number, and the pressure loss coefficient will now be described. The application of the analogy between heat and mass transfer will also be discussed.

The per-module mass transfer $\dot{m}$ per unit time and unit area was evaluated from the measured mass loss, the duration time of the data run, and the surface area of the module exposed to the airflow. With $\dot{m}$ as input, the mass transfer coefficient K follows from its definition

$$K = \dot{m}/(\rho_{nw} - \rho_{nb}) \tag{3}$$

in which ρ_{nw} and ρ_{nb} respectively denote the naphthalene vapor densities at the surface of the module and in the bulk flow. The former was calculated from successive application of the Sogin vapor pressure–temperature relation and the perfect gas law, while the latter is zero in the present experiments.

As noted earlier, the major emphasis in the presentation of results will be the identification of the effects of missing modules and/or the presence of a barrier. To accomplish this objective, the mass transfer coefficients will, in the main, be presented in the form of a ratio K/K^*. In this ratio, K denotes the coefficient value corresponding to missing modules and/or a barrier, while K^* is the fully developed coefficient in the completely populated array without barriers. Both K and K^* correspond to the same Reynolds number.

The aforementioned K/K^* ratio is, of course, dimensionless, and its use circumvents the issue of selecting a characteristic length. A length scale must, however, be selected in reporting the dimensionless K values for the baseline case (i.e., the fully populated array without barriers). In view of the fact that four dimensions (L, t, S and H) are needed to characterize the array, the choice of a characteristic length is somewhat arbitrary. Here, the module planform length L is used, so that the per-module Sherwood number (the counterpart of the Nusselt number) is given by

$$Sh = KL/\mathscr{D}. \tag{4}$$

The diffusion coefficient $\mathscr{D}$ was evaluated indirectly via the Schmidt number $Sc = \nu/\mathscr{D}$, with $Sc = 2.5$ for the naphthalene–air system [3]; ν is the kinematic viscosity of air.

There is also an ambiguity in the selection of a Reynolds number, since the free flow area varies periodically throughout the array. If the gap of height H between the modules and the opposite wall of the channel (see Fig. 1) is regarded as the main passage for fluid flow, then a characteristic velocity may be evaluated from

$$\rho V = \dot{w}/A_H \tag{5}$$

in which A_H is the flow cross-section associated with the gap height H and $\dot{w}$ is the rate of airflow through the system. Consistent with the foregoing, H will be selected as the characteristic dimension in the Reynolds number. Thus,

$$Re = \rho V H/\mu = \dot{w}/\mu(A_H/H). \tag{6}$$

The quantity (A_H/H) is the spanwise width of the flow passage. Since the geometrical factors appearing in equation (6) were fixed throughout the present experiments, Re played the role of a dimensionless airflow rate.

Attention will now be turned to the format to be used in the presentation of the pressure drop results. For the baseline case (no missing modules and no barriers), a periodic fully developed regime is established downstream of a hydrodynamic development region. In the fully developed regime, the per-row pressure drop Δp_{row} is constant; it will be presented in ratio form as

$$\Delta p_{row}/\tfrac{1}{2}\rho V^2 \tag{7}$$

where, from equation (5), $\rho V^2 = (\dot{w}/A)^2/\rho$ and ρ was evaluated at the mean pressure in the array of modules.

The presence of a barrier gives rise to a substantial additional pressure drop relative to the pressure drop in the no-barrier case. This incremental pressure drop Δp_{incr} will also be reported in dimensionless form

$$\Delta p_{incr}/\tfrac{1}{2}\rho V^2 \tag{8}$$

where, again, $\rho V^2 = (\dot{w}/A)^2/\rho$, but with ρ corresponding to the pressure just upstream of the barrier.

As a final item in this section, the heat–mass transfer analogy will be briefly discussed. According to the analogy, if Nu and Sh are represented as

$$Nu = f(Re, Pr, \chi_i), \quad Sh = f(Re, Sc, \chi_i) \tag{9}$$

then the functions f are the same in both representations (χ_i denotes geometrical parameters).

In the correlation of heat and mass transfer data, it is common to specialize equation (9) as

$$Nu = Pr^m g(Re, \chi_i), \quad Sh = Sc^m g(Re, \chi_i) \tag{10}$$

so that

$$Nu = (Pr/Sc)^m Sh. \tag{11}$$

For tube bank arrays, Zukauskas [4] recommends $m = 0.36$. With $Pr = 0.7$ for heat transfer in air and $Sc = 2.5$ for naphthalene diffusion in air, equation (11) becomes

$$Nu = 0.632\, Sh \tag{12}$$

which enables the present Sherwood numbers to be transformed to Nusselt numbers for heat transfer in a geometrically similar airflow system.

Eckert [5] has examined the requisite conditions for the validity of the analogy on theoretical grounds, and empirical testimony has been provided by laboratory experiments at Minnesota.

RESULTS AND DISCUSSION

The presentation of results will begin with the heat (mass) transfer characteristics of the baseline case (no missing modules and no barriers) and then goes on to missing modules, implanted barriers, and combinations of missing modules and implanted barriers. The pressure drop information will close out the presentation.

Baseline case

The row-by-row distribution of the per-module Sherwood number is shown in Fig. 3 for Reynolds numbers of 2000, 3700 and 7000. For all Reynolds numbers, there is a common pattern wherein the highest Sherwood number is attained in the first row and, with increasing downstream distance, the Sherwood number decreases at first but then attains a row-independent constant value. In particular, the Sherwood number is seen to be constant for the 5th and all subsequent rows, and these rows may be regarded as constituting the fully developed region.

A horizontal line corresponding to the average value of the Sherwood number data in the fully developed region is shown in Fig. 3 for each Reynolds number. These average Sh values are 35.34, 54.30 and 87.15, respectively for $Re = 2000$, 3700 and 7000. A least squares fit of these numerical values yields

$$Sh = 0.148\, Re^{0.72} \tag{13}$$

with an extreme deviation of 1%. With this and with the aid of equation (12), the fully developed Nusselt numbers for heat transfer (to air) can be represented as

$$Nu = 0.0935\, Re^{0.72} \tag{14}$$

For the modules situated in the entrance region, the Nusselt numbers can be obtained from

$$Nu_{ent} = (Sh_{ent}/Sh_{fd})Nu_{fd} \tag{15}$$

where subscripts ent and fd have been appended to clearly distinguished the entrance and fully developed regions.

Missing modules

The first set of results corresponds to the effects of a single missing module on the per-module heat (mass) transfer coefficient at positions which are uninfluenced by the entrance region. As noted earlier, the results are presented in the form of a ratio K/K^* ($= h/h^*$). The numerator is the heat or mass transfer coefficient at a particular location when there is a missing module somewhere in the array, while the denominator is the coefficient at the same location when there are no missing modules. Since the selected location of interest is in the fully developed region, K^* and h^* can respectively be obtained from equations (13) and (14).

To achieve a compact presentation of the extensive set of data that was collected, a format illustrated in the upper part of Fig. 4 is adopted. A plan view of a portion of the array is shown there. The module at which the heat transfer coefficient is being monitored is designated by a speckled pattern, and there is a missing module (i.e. an empty space) two rows upstream of the module of interest. The three numbers inscribed in the speckled module are the K/K^* and h/h^* ratios at that site which relate to the designated missing module. As indicated at the extreme right of the array, these ratios correspond respectively to Reynolds numbers of 2000, 3700 and 7000.

This presentation is entirely satisfactory if the only case to be considered is that pictured in the diagram. Suppose, however, that it is desired also to record the

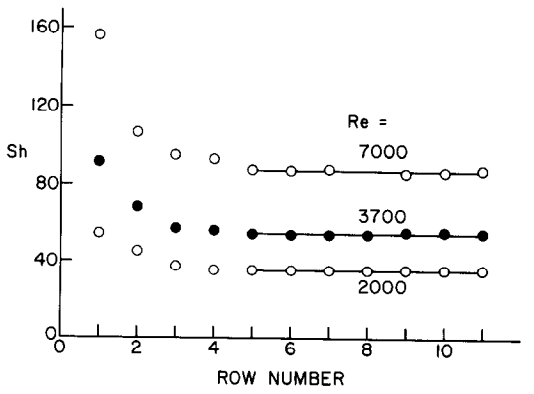

FIG. 3. Row-by-row distributions of the per-module Sherwood number for the fully populated array without barriers.

K/K^* and h/h^* ratios at the speckled module corresponding to a single missing module at a site that is three rows upstream of it. Clearly, there is no available space in the speckled module to inscribe the ratios for this case, since the space is fully occupied by the ratios for the prior case. This difficulty of presentation becomes more and more severe as K/K^* and h/h^* ratios at the speckled module are measured for a large range of sites of a single missing module.

The resolution of the difficulty is illustrated schematically in the figure. As seen there, the K/K^* and h/h^* ratios at the speckled module are transferred to the site of the missing module whose absence gave rise to the values of the ratios.

With the use of this format, results for the K/K^* and h/h^* ratios at the speckled module are presented in the lower part of Fig. 4 for a large number of different sites of a single missing module. From an overall inspection of these results, it is seen that the tabulated ratios are in excess of one, except for a few 0.98 and 0.99 values which, in all likelihood, are not significant because of the estimated 2% uncertainty in the data. It follows, therefore, that if there is a missing module in the array, the heat transfer coefficients at other modules situated in the general neighborhood are larger than when there are no missing modules. This qualitative finding is, in itself, of considerable practical importance.

The greatest enhancement, on the order of 40%, occurs when the missing module is just upstream of the module at which the heat transfer coefficient is being monitored. The extent of the enhancement diminishes when the site of the missing module is located farther and farther upstream of the module of interest, with the rate of diminution being relatively rapid for the highest Reynolds number and substantially slower for the lowest Reynolds number. In general, upstream-located missing modules which lie in the same column as the module of interest yield greater enhancements at low Reynolds numbers than at high Reynolds numbers. This is because a low Reynolds number flow penetrates the cavity created by the missing module while a high Reynolds number flow tends to skim over the cavity. As a consequence, the low Reynolds number flow is more disturbed when there is a missing module than is a high Reynolds number flow.

A missing module situated either at the side or just downstream of the module of interest causes a markedly smaller enhancement than that caused by a missing module that is just upstream. There is no effect when a missing module is located two or more rows downstream of the monitored module. A missing module located at the side and upstream of the monitored module creates a modest effect over a range of two or three rows.

The next set of results pertains to the effect of a pair

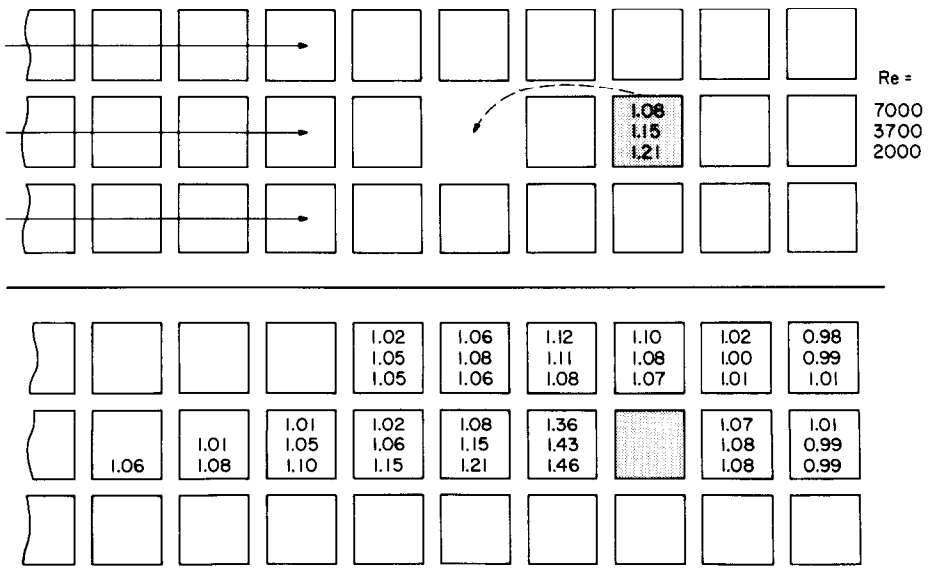

FIG. 4. Effect of a missing module on the mass and heat transfer coefficients at neighboring modules. Upper diagram: illustration of the presentation format; lower diagram: presentation of the K/K^* and h/h^* ratios.

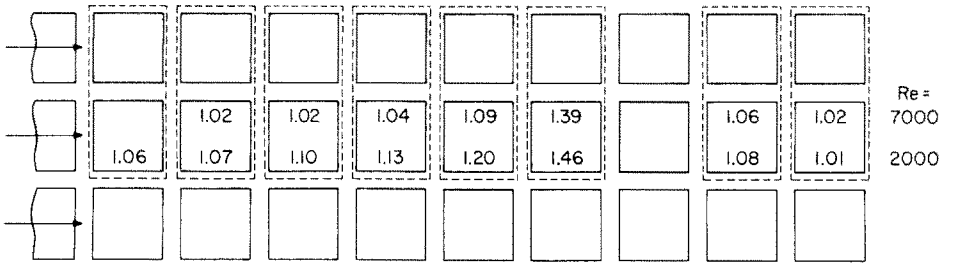

FIG. 5. Effect of a pair of side-by-side missing modules on the mass and heat transfer coefficients at neighboring modules. The presented values are the K/K^* and h/h^* ratios.

of missing modules whereby the two missing modules in each pair are side by side in a given row. Attention is focused on the values of K/K^* and h/h^* at a module of interest and on the response of these values to the location of the site of the missing module pair. With regard to the graphical presentation of results, it is impractical, as before, to inscribe the numerical values of the K/K^* and h/h^* ratios atop the site of the module of interest. Rather, these ratios are recorded at the site of the missing module pair whose absence gave rise to the values.

The results are presented in Fig. 5, whose format is modeled after that of the lower diagram of Fig. 4. The module at which the heat transfer coefficients are being monitored is shown speckled, while the respective sites of the various missing module pairs are delineated by dashed lines. The K/K^* and h/h^* values associated with each missing pair are inscribed in the space associated with the centermost module of the pair. Results are given for $Re = 2000$ and 7000, as indicated in the figure.

It is instructive to compare the numerical values corresponding to the missing module pairs of Fig. 5 with the values displayed in Fig. 4 for a single missing module situated in-line with respect to the module of interest. Such a comparison reveals that the two sets of values are nearly identical, with deviations that are more or less within the accuracy of the experiments. Thus, it appears that the in-line missing module in a spanwise group of missing modules plays the dominant role in shaping the degree of heat transfer enhancement at a module situated in a neighboring row.

Implanted barriers

The effect of an implanted barrier on the heat or mass transfer coefficients at a module of interest will now be examined. The results will again be presented in terms of the K/K^* and h/h^* ratios, where K and h refer to the coefficients at the module of interest with the barrier in place, and K^* and h^* are the coefficients at the same module when there is no barrier. As before, the latter can be calculated from equations (13) and (14).

In the experiments, the barrier was implanted downstream of the entrance region. As noted earlier and quantified by equations (2) and (2a), two barrier heights were employed. The results for the lower of the

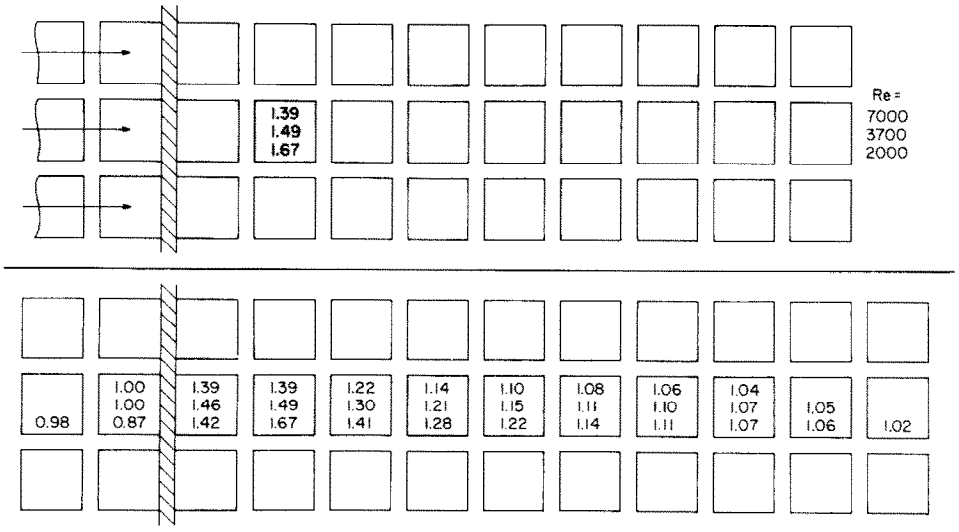

FIG. 6. Effect of an implanted barrier of height $(b - t)/H = \frac{1}{5}$ on the mass and heat transfer coefficients at neighboring modules. Upper diagram: illustration of the presentation format; lower diagram: presentation of the K/K^* and h/h^* ratios.

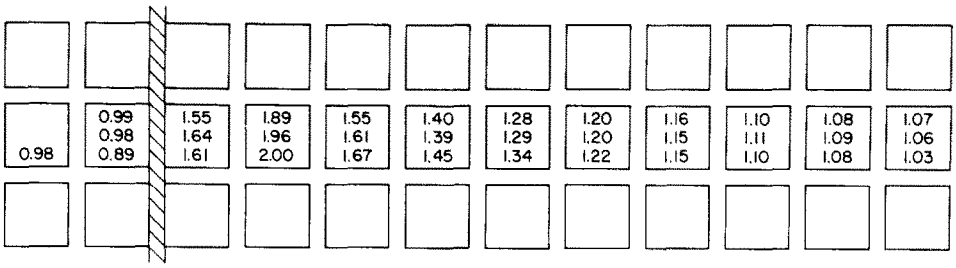

FIG. 7. Effect of an implanted barrier of height $(b - t)/H = \frac{2}{5}$ on the mass and heat transfer coefficients at neighboring modules. The presented values are the K/K^* and h/h^* ratios.

barriers are presented in Fig. 6, and those for the higher barrier are given in Fig. 7.

Figure 6 is subdivided into upper and lower diagrams. The purpose of the upper diagram is to illustrate the format of the presentation. As seen there, the module at which the heat transfer coefficient is being monitored is shown speckled. The K/K^* and h/h^* values at that module are inscribed directly in the module for the three Reynolds numbers investigated. This same trio of numbers is shown in the corresponding site in the lower diagram. The lower diagram is a composite showing the barrier-related K/K^* and h/h^* values at each of the modules.

From the figure, it is seen that the barrier effectively fulfils its function as a heat transfer enhancement device. The greatest enhancements occur in the second row downstream of the barrier, where the heat transfer coefficients are 67, 49 and 39% higher than those for the no-barrier case, respectively for Reynolds numbers of 2000, 3700 and 7000. The fact that the transfer coefficients at the second-row modules exceed those in the first row indicates that the reattachment of the flow, which lifts off due to the presence of the barrier, takes place in the 2nd row. With increasing downstream distance, the extent of the enhancement drops off, but even at the 5th row the coefficients are 22, 15 and 10% higher than their no-barrier counterparts. At the 8th row, the increases in the coefficient are 5% or less.

In general, the largest percentage increases in the coefficient occur at the lowest Reynolds number, which is consistent with previous work which shows that low Reynolds number flows are more susceptible to disturbances that are high Reynolds number flows. It is also seen from Fig. 6 that the barrier-induced enhancements persist to greater downstream distances at lower Reynolds numbers. By this same token, the upstream effect of the barrier is also accentuated at low Reynolds numbers, with the result that at the module immediately upstream of the barrier, there is a reduction in the transfer coefficient in excess of 10% at $Re = 2000$.

Attention may now be turned to Fig. 7, which shows the K/K^* and h/h^* ratios for the higher of the two barriers investigated. The structure of this figure is identical to that of the lower diagram of Fig. 6.

Comparison of the results of the two figures shows that the higher barrier provides substantially greater and longer-lived enhancement. The maximum enhancement continues to occur in the 2nd row downstream of the barrier, but even more decisively than before. With the barrier in place, the 2nd row heat transfer coefficients are about double for the no-barrier case. It is interesting to note that the enhancement in the 3rd row exceeds that of the 1st row, testifying to the long lift-off trajectory imparted to the airflow by the higher barrier.

Enhancements in the 30% range are in evidence in the 5th row, and 5% enhancements persist as far downstream as the 10th row. Another noteworthy feature of the results for the higher barrier is their lesser dependence upon the Reynolds number.

It is evident that higher barriers are advantageous from the standpoint of heat transfer enhancement. There is, however, a severe pressure drop penalty, the magnitude of which will be presented shortly.

Implanted barriers and missing modules

Experimental results will now be reported for the situation in which there is both a barrier and a missing module in the array. Three categories of barrier–missing module configurations were investigated, and these are illustrated in Fig. 8. In all cases, both the missing module and the monitored module are situated downstream of the barrier, since it has already been demonstrated that a barrier has virtually no effect on modules situated upstream of it. Correspondingly,

Table 1. K/K^* and h/h^* ratios: implanted barriers and missing modules†

	A		B		C	
Row	2000	7000	2000	7000	2000	7000
1			1.66	1.65	1.58	1.53
2	2.16	1.97	1.98	1.87	2.03	1.93
3	1.99	1.78	1.67	1.59	1.73	1.61
4	1.68	1.60	1.50	1.43	1.50	1.48
5	1.57	1.53				
6	1.57	1.52				
7	1.55	1.53				
8	1.53	1.55				
9	1.51	1.47				
10	1.50	1.42				

Barrier height, $(b - t)/H = 2/5$.
†Configurations illustrated in Fig. 8.

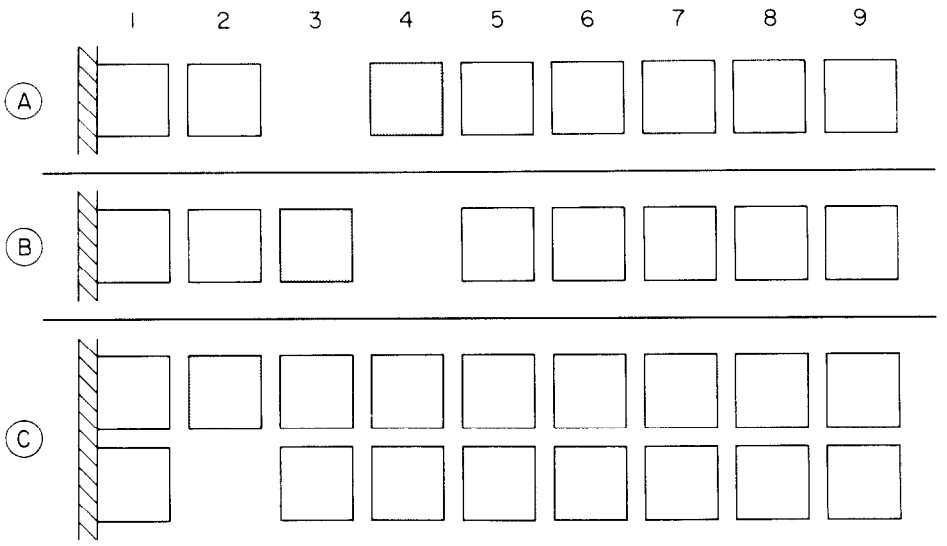

FIG. 8. Categories of barrier–missing module configurations for which experiments were performed.

as shown in Fig. 8, the numbering system used to identify the rows of modules begins at the barrier. That is, the row immediately downstream of the barrier is row 1, the next is row 2, etc.

The three categories of barrier–missing module configurations are designated as A, B and C in Fig. 8. In category A, the missing module is located immediately upstream of the speckled module at which the heat transfer characteristics are being monitored, whereas in category B the missing module is immediately downstream of the monitored module. In the third category, C, the missing module is just to the side of the monitored module.

The barrier implanted during this set of experiments is the taller of the two used in the experiments reported earlier in the paper. For this barrier, $(b - t)/H = \frac{2}{5}$, that is, the barrier blocks 40% of the gap between the modules and the opposite wall. The barrier was positioned downstream of the entrance region.

Data runs were made for Reynolds numbers of 2000 and 7000. As before, the results are presented in terms of the K/K^* and h/h^* ratios. The numerator of the ratio is the value of the transfer coefficient at the monitored module when there is a barrier and a missing module in the array; the denominator represents the transfer coefficient for fully developed conditions in a fully populated array without barriers.

The K/K^* and h/h^* ratios are presented in Table 1 under columns A, B, and C which respectively correspond to the A, B and C categories of Fig. 8. For each category, the results for the two Reynolds numbers are listed side by side. In interpreting the tabulated information, it will be necessary only to focus on one of the Reynolds numbers, for instance, $Re = 2000$, since the same trends apply for both Reynolds numbers.

Consider first the results for category A. In this regard, it is useful to note from Fig. 4 that in the absence of a barrier, a missing module located just upstream of a monitored module gives rise to K/K^* and h/h^* ratios of 1.46 when $Re = 2000$. It is also useful to take note of the ratios listed in Fig. 7 for monitored modules situated downstream of a barrier. With this background, it may be seen from the second column of Table 1 that the separate enhancements due to a

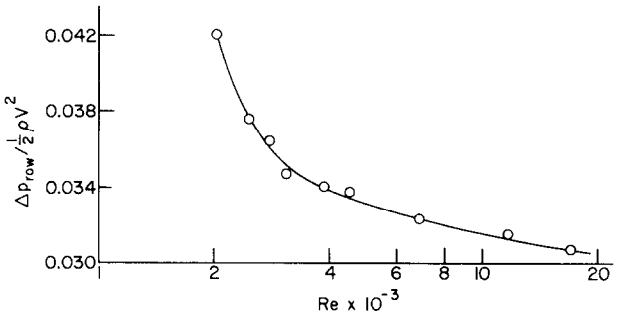

FIG. 9. Per-row pressure drop for the fully populated array without barriers.

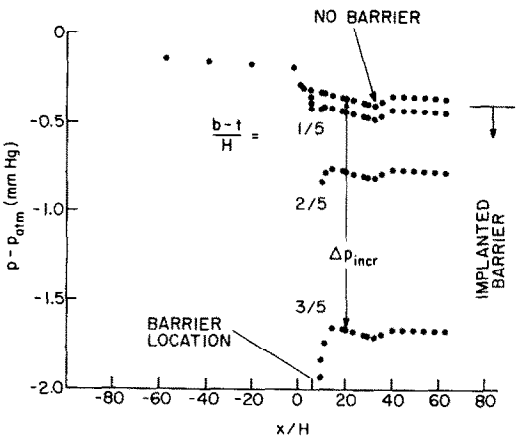

FIG. 10. Axial pressure distributions for arrays with and without barriers, $Re = 6900$.

missing module and to a barrier are not directly additive when there is both a missing module and a barrier in the array. However, the two effects are, in all cases, mutually reinforcing.

Near the barrier, the already impressive barrier-related enhancement is moderately increased due to the missing module. Well downstream of the barrier, the tabulated ratios approach the value 1.46 which pertains to a missing module without barriers.

For category B, it was found that in the near-barrier region, a missing module positioned downstream of the monitored module has little effect on the K/K^* and h/h^* ratios which are induced by the barrier. A similar observation applies to a side-positioned missing module. The absence of added enhancement in the near-barrier region, which is the region of interest when a barrier is implanted, prompted the truncation of the experiments after the fourth row.

Pressure losses

The per-row pressure drop for the baseline case (no missing modules and no barriers) is plotted in dimensionless form as a function of the Reynolds number in Fig. 9. The quantity $\frac{1}{2}\rho V^2$ used to normalize the pressure drop is discussed in the text following equation (7). As noted earlier, the per-row pressure drop (i.e. that given in Fig. 9) is independent of position in the array in the fully developed region.

From the figure, it is seen that the behavior of the dimensionless pressure drop is similar to that of the friction factor for pipe flow, i.e. a monotonic decrease with increasing Reynolds number. There is no evidence of laminar–turbulent transition which reinforces the perception that the flow is turbulent for all of the Reynolds numbers investigated.

When a barrier is implanted in the array, it gives rise to a substantial pressure loss relative to the baseline case. Figure 10 has been prepared to illustrate the incremental pressure drop due to the presence of a barrier. The figure displays the measured pressure distribution along the entire length of the experimental apparatus for the baseline case and for three different heights of an implanted barrier. The data shown in the figure correspond to a Reynolds number that is just under 7000.

The linear pressure distribution in the module-free inlet section ($x < 0$) is seen to be common to all of the configurations investigated, as is to be expected since the Reynolds number is common to all. The array of modules begins at $x = 0$, and there is an abrupt pressure drop at that point, once again common to all cases, as the flow enters the array and accommodates to a decrease in the free-flow area. For the baseline case, the flow traverses the array along an essentially linear pressure distribution and then recovers pressure as it leaves the array and encounters the enlarged free-flow area of the exit length. In the exit length, a linear decrease of pressure is re-established.

The axial position of the barrier, which is implanted between the 3rd and 4th rows, is illustrated on the abscissa of Fig. 10. As the flow crosses the barrier, it pinches together, and this gives rise to a sharp pressure drop whose magnitude increases as the barrier height increases. Just downstream of the barrier, as the flow expands from its pinched condition and fills the available cross-section, a pressure recovery takes place which, once again, is greater for taller barriers. The recovery is, however, rather small compared with the initial pressure drop caused by the barrier, and a substantial barrier-related net pressure loss remains. Once the flow fills the free-flow area of the array, the subsequent pressure events are the same as those for the baseline case.

The incremental pressure drop Δp_{incr} associated with the tallest barrier is identified in Fig. 10, and an identical approach is used to determine Δp_{incr} for the other barriers. As seen there, Δp_{incr} is evaluated subsequent to the pressure recovery which takes place just downstream of the barrier and it is, therefore, the net barrier-related pressure loss. Numerical values of Δp_{incr} have been determined for several Reynolds numbers in the range between 2000 and 7000 for each of the barrier heights shown in Fig. 10.

The dimensionless pressure loss results are listed in Table 2, where the velocity head has been used in the non-dimensionalization [see equation (8) and the related text]. To provide perspective for these results, it may be noted from Fig. 9 that for the no-barrier case,

Table 2. Barrier-related incremental pressure losses, $\Delta p_{incr}/\frac{1}{2}\rho V^2$

	$(b-t)/H$		
Re	1/5	2/5	3/5
2020	0.45	2.4	7.9
3050	0.46	2.3	7.6
4550	0.43	2.3	7.3
6900	0.42	2.3	7.1

$\Delta p_{row}/\frac{1}{2}\rho V^2 \sim 0.32$–$0.042$ for the Reynolds numbers of Table 2. Thus, even for the lowest barrier investigated, the incremental pressure loss is comparable to the pressure drop for 10 or more rows of an array without barriers. The intermediate barrier gives rise to a 5-fold increase in the pressure loss relative to that for the lowest barrier, and an additional 3-fold increase occurs between the intermediate and the tallest barriers. The pressure loss for the latter appeared to be too great to warrant an exploration of the heat transfer characteristics, thereby explaining the absence of these results from the presentation made earlier in the paper.

If Table 2 is considered in conjunction with Figs. 6 and 7, it is seen that the higher pressure losses incurred with taller barriers are compensated by somewhat higher heat transfer coefficients. The ultimate decision as to whether the larger losses are tolerable depends upon the criticalness of the specific cooling problem in question.

As a final comment with respect to Table 2, it may be observed that for a fixed barrier height, the dimensionless pressure loss is a weak function of the Reynolds number. This finding indicates that the losses are primarily due to inertial effects.

CONCLUDING REMARKS

The research reported here appears to be the first systematic experimental investigation of the heat transfer and pressure drop characteristics of arrays of heat generating, rectangular modules that are commonly encountered in electronic equipment. Experiments were performed with fully populated arrays, arrays in which there are missing modules, arrays where barriers are implanted to obtain heat transfer enhancement, and arrays in which there is both a missing module and a barrier. Air was the heat transfer medium in all of the experiments.

For the fully populated array without barriers, row-independent (fully developed) heat transfer coefficients were encountered for the 5th and all subsequent rows. The fully developed Nusselt numbers are correlated as a function of Reynolds number by equation (14).

If there is a missing module in the array, the heat transfer coefficients at other modules situated in the general neighborhood are larger than when there are no missing modules. The greatest enhancement, on the order of 40%, occurs when the missing module is just upstream of the module at which the heat transfer coefficient is being monitored. The largest percentage enhancements are encountered at lower Reynolds numbers.

Results were also obtained for the case in which there are two missing modules side by side in a given row of the array. The heat transfer enhancement associated with such a pair of missing modules is nearly the same as that induced by a single missing module.

The implantation of a barrier in the array is shown to be an effective means of heat transfer enhancement. The greatest enhancements occur in the second row downstream of the barrier, with the largest percentage increases in evidence at the lower Reynolds numbers. Enhancement is further increased with increases in barrier height. For the operating conditions investigated here, the largest barrier-related enhancement was a factor of two.

In the experiments involving both a barrier and a missing module, both the missing module and the monitored module were positioned downstream of the barrier. The enhancing effects of a missing module and a barrier were found to be mutually reinforcing when the missing module is upstream of the monitored module. However, there is little reinforcement when the missing module is located either to the side or downstream of the monitored module.

Pressure distributions were measured in arrays with and without a barrier. For the lowest barrier investigated, the barrier-induced pressure drop was approximately equal to that for 10 rows of an array without a barrier; the pressure loss for the intermediate barrier was equivalent to that for about 60 rows in a barrier-free array.

REFERENCES

1. A. D. Kraus, *Cooling Electronic Equipment*. Prentice-Hall, Englewood Cliffs, NJ (1965).
2. A. E. Bergles, The evolution of cooling technology for electrical equipment and electronic devices. In *Directions of Heat Transfer in Electronic Equipment* (edited by A. D. Kraus, A. E. Bergles, and J. C. Mollendorf). Atlanta, Georgia (1977).
3. H. H. Sogin, Sublimation from discs to air streams flowing normal to their surfaces, *Trans. ASME* **80**, 61–71 (1958).
4. A. A. Zukauskas, Heat transfer from tubes in crossflow. In *Advances in Heat Transfer*. Vol. 8. Academic Press, New York (1972).
5. E. R. G. Eckert, Analogies to heat transfer processes. In *Measurements in Heat Transfer*. Hemisphere, Washington D.C. (1976).

CARACTERISTIQUES DE TRANSFERT THERMIQUE ET DE PERTE DE CHARGE DANS DES ARRANGEMENTS DE MODULES RECTANGULAIRES D'EQUIPEMENTS ELECTRONIQUES

Résumé—Une étude expérimentale concerne le transfert thermique et la perte de charge d'un écoulement dans des arrangements de modules rectangulaires, sources de chaleur, appliqués sur une paroi plane rectangulaire. Des expériences portent sur des lignes complètes, des lignes où manquent des modules, des lignes où sont implantées des barrières pour obtenir un accroissement du transfert thermique, et des lignes dans lesquelles il y a à la fois un module manquant et une barrière. Pour les rangées complètes sans barrière, on constate des coefficients de transfert thermique indépendants de la profondeur (pleinement développés) à partir de la cinquième rangée. Quand il manque un module dans la ligne, les coefficients de transfert dans les modules voisins sont augmentés avec un plus grand accroissement (environ quarante pour cent) lorsque le module manquant est juste en amont du module considéré. L'accroissement dû à une paire contiguë de modules manquants diffère très peu de celui induit par un seul module manquant. L'implantation d'une barrière dans la ligne est effectivement favorable, avec le plus grand effet (environ un facteur égal à deux) dans la seconde rangée en aval de la barrière mais avec un accroissement résiduel qui persiste considérablement loin en aval. Sous certaines conditions, les effets d'accroissement d'un module manquant et d'une barrière se renforcent mutuellement. Des distributions de pression sont mesurées dans les lignes avec ou sans barrières et on identifie les pertes de pression induites par la barrière.

VERHALTEN VON WÄRMEÜBERGANG UND DRUCKABFALL BEI ANORDNUNGEN VON RECHTECKIGEN MODULN IN ELEKTRONISCHEN GERÄTEN

Zusammenfassung—Umfangreiche experimentelle Untersuchungen wurden angestellt, um den Wärmeübergang und Druckabfall einer Luftströmung bei Anordnungen von wärmeerzeugenden rechteckigen Moduln, die an einer Wand eines flachen Rechteckkanals angebracht sind, zu bestimmen. Versuche mit voll bestückten Feldern, Feldern, in denen Moduln entfernt worden waren, Feldern, in die Barrieren eingebaut waren, um eine Erhöhung des Wärmeübergangs zu erreichen, und mit Feldern, in denen sowohl Moduln entfernt als auch Barrieren eingebracht waren, wurden durchgeführt. Für voll besetzte Felder ohne Barrieren wurden für die fünfte und alle nachfolgenden Reihen reihenunabhängigeWärmeübergangskoeffizienten gefunden. Fehlt ein Modul in einer Anordnung, so steigt der Wärmeübergangskoeffizient bei benachbarten Moduln an, wobei der größte Anstieg (über 40 Prozent) dann beobachtet wird, wenn der fehlende Modul stromaufwärts direkt vor dem betrachteten Modul liegt. Die Erhöhung, welche durch zwei fehlende nebeneinanderliegende Moduln verursacht wird, unterscheidet sich nur geringfügig von der bei nur einem fehlenden Modul. Die Anbringung einer Barriere in einem Feld hat sich als wirksame Methode zur Erhöhung des Wärmeübergangs erwiesen. Der größte Einfluß (mit einem Faktor über 2) tritt dabei in der zweiten Reihe stromabwärts der Barriere auf, wobei aber auch wesentlich weiter stromabwärts eine restliche Erhöhung erhalten bleibt. Weiter wurde gefunden, daß sich die Effekte eines fehlenden Moduls und einer Barriere unter bestimmten Bedingungen gegenseitig verstärken. Um den durch eine Barriere entstehenden Druckverlust zu ermitteln, wurden Druckverteilungen in Feldern mit und ohne Barriere gemessen.

ХАРАКТЕРИСТИКИ ТЕПЛОПЕРЕНОСА И ПЕРЕПАДА ДАВЛЕНИЯ В РЕШЕТКАХ ПРЯМОУГОЛЬНЫХ МОДУЛЕЙ, ИСПОЛЬЗУЕМЫХ В ЭЛЕКТРОНИКЕ

Аннотация — Выполнено всестороннее экспериментальное исследование теплопереноса и перепада давления при обтекании воздухом решетки тепловыделяющих прямоугольных модулей, помещенных вдоль одной стенки плоского прямоугольного канала. Эксперименты проводились с заполненными решетками; с решетками без нескольких модулей; решетками с перегородками для интенсификации теплообмена и с решетками без одного модуля и с одной перегородкой. Для заполненных решеток без перегородок коэффициенты теплопереноса (полностью развитого) переставали зависеть от номера ряда для пятого и следующих рядов модулей. В решетках с одним пропущенным модулем коэффициенты теплопереноса для модулей в смежных зонах возрастают, причем теплообмен максимально интенсифицируется (около 40%), когда зазор расположен вверх по потоку от пропущенного модуля. При отсутствии пары рядом расположенных модулей величина теплообмена мало чем отличается от вышерассмотренного случая. Показано, что перегородка значительно (почти в 2 раза) усиливает теплообмен особенно во втором ряду модулей вниз по потоку от перегородки, и это усиление ощущается и в последующих рядах. Найдено, что в некоторых условиях использование перегородки и изъятие модуля взаимно интенсифицируют теплообмен. Измерены распределения давления в решетках с перегородками и без них и определены потери давления, обусловленные перегородками.